Structure and Spectroscopy of Criegee Intermediates in Gas- and Aqueous Environments

Cangtao Yin, Meenu Upadhyay and Markus Meuwly*

Department of Chemistry, University of Basel, Klingelbergstrasse 80, CH-4056 Basel,
Switzerland

E-mail: m.meuwly@unibas.ch

Abstract

The dynamics and spectroscopy of the small (H₂COO) and large (CH₃CHOO) Criegee intermediates (CIs) in the gas phase, inside/on water droplets, on amorphous solid water (ASW) and in bulk water are investigated using validated energy functions. For both species, facile diffusion between surface and inside positions for water droplets are found whereas on amorphous solid water at low temperatures (50 K) no surface diffusion is observed on the multiple-nanosecond time scale. This is at variance with other species, such as CO or NO on ASW. The infrared spectroscopy of both CIs in contact with an aqueous environment leads to shifts of the spectral features on the order of a few to a few tens of cm⁻¹, depending on the vibrational mode considered. This is consistent with Stark-induced spectral shifts for small molecules in protein environments. However, the spectroscopy of both CIs in contact with water droplets does not depend on the positioning relative to the droplet (inside vs. surface).

Introduction

The nature and phase of chemical environments can play decisive roles for the structure, spectroscopy, reactivity and other relevant chemical properties of solutes. A particularly notable example constitute chemical reactions on the surface of droplets which has been a hotly debated subject over the past decade. Another area where specific effects can be expected concerns the spectroscopic response of solutes in different chemical environments. This arises in atmospheric and interstellar chemistry where adsorbates experience varying environments depending on the local properties of the medium. For example, adsorbates on amorphous solid water have been found to follow non-Arrhenius diffusion due to surface roughness.¹

Infrared (IR) and vibrational spectroscopy is a powerful non-destructive technique to characterize systems in the gas- and condensed phase. For example, IR spectra can provide information to infer structure from spectroscopic responses. This has, for example, been used to determine the metastable structure of free carbon monoxide in the active site of myoglobin.²⁻⁹ Due to the strong inhomogeneous electric fields inside a protein, spectral responses shift and split as a consequence of changes in the structure. This has also been used to relate ligand binding strength and frequencies of a spectroscopic reporter such as cyanolated benzenes.^{10,11}

Aqueous (micro)droplets and aerosols are environments relevant to atmospheric chemistry and laboratory-based experiments. The strong electric fields at the interfaces of aqueous droplets can influence the spectroscopy of guest molecules and their reactivity. $^{12-15}$ Spectroscopically, stimulated Raman excited fluorescence microscopy has been used to measure a 5 cm⁻¹ red shift for the -CN stretch vibration in rhodamine 800 between the bulk and the microdroplet environment. 12 In addition, chemical reactions in and on water droplets have recently been found to be accelerated by orders of magnitudes compared with the same reactions in bulk water. $^{13-15}$ How exactly microdroplets lead to such accelerations at a molecular level is still debated but it is suspected that a number of factors contribute to this observation: solvent evaporation from the droplet, confinement of the reagents, the electric fields $(10^7 \text{ V/cm}$, surface potential $3.63 \text{ V})^{16}$ at the air-solvent interface, droplet size, or molecular orientation at the interface to name a few. On the other hand, for a Diels-Alder reaction that occurs readily in bulk solvent it was found that no product was formed at all. 14 This is consistent with work on pyruvic acid which reported different chemistry depending on whether the photochemistry occurred in aqueous bulk environment or at the air-water interface. 16

Criegee intermediates (CIs), generated during alkene ozonolysis, are highly reactive carbonyl oxides that play crucial roles in atmospheric oxidation, notably in the conversion of SO₂ to

H₂SO₄ and the formation of secondary organic aerosols (SOA).¹⁷ Generally speaking, CIs are generated from alkene ozonolysis through a 1,3-cycloaddition of ozone across the C=C bond to form a primary ozonide which then decomposes into carbonyl compounds and energized carbonyl oxides, known as CIs.¹⁸ Such highly energized intermediates rapidly undergo either unimolecular decay to hydroxyl radicals¹⁹ or collisional stabilization.²⁰ Stabilized Criegee intermediates can isomerize and decompose into products including the OH radical, or undergo bimolecular reactions with water vapor, SO₂, NO₂ and acids.^{21,22}

Aerosols can substantially influence CI chemistry by providing surfaces and aqueous microenvironments that promote adsorption, stabilization, or enhanced reactions with water, SO₂ and organics. ^{23,24} Such heterogeneous or interfacial processes can alter CI lifetimes and branching ratios, affecting radical budgets and oxidation capacity. For instance, solvation or hydrogen bonding within droplets may accelerate CI hydration or rearrangement to peroxides, while reactions at aerosol surfaces may enhance sulfuric acid formation and SOA growth. ²⁵ Consequently, aerosols act not only as sinks but as active participants that modulate Criegee intermediate reactivity and their broader atmospheric impacts.

The present work focuses on the adsorption and spectroscopic properties of the two smallest CIs: H₂COO and syn-CH₃CHOO. First, the methods used are described. This is followed by results on the structural characterization of the CIs in the various environments. Next, the infrared spectra of the two CIs depending on the environment are analyzed. Finally, conclusions are drawn.

Methods

Molecular Dynamics Simulations

All molecular dynamics (MD) simulations were carried out with the CHARMM and py-CHARMM suite of codes.^{26–29} For both systems studied here, H₂COO and *syn*-CH₃CHOO, two different and validated reactive PESs from previous work are available.^{30–33} The PESs are based on multi-state adiabatic reactive MD (MS-ARMD)³⁴ and a neural network-based representation for which the PhysNet architecture was used.³⁵

Simulations using MS-ARMD were run using CHARMM, whereas for the mixed machine learning/molecular mechanics (ML/MM) MD simulations the pyCHARMM code was employed. In all simulations the systems were first heated and equilibrated at the target temperature before production simulations, 2 ns in length, were carried out. Four different system setups were considered: the CIs in the gas phase, CIs adsorbed on amorphous solid water (ASW), CIs on and within water droplets, and finally CIs in bulk water. In all simulations the time step was $\Delta t = 0.1$ fs.

For CIs adsorbed on water a previously generated setup for the ASW was used. 1,36 The initial ASW structure was generated as described previously. 36 Starting from a TIP3P 37 water box (31 × 31 × 50 Å 3), equilibrated at 300 K, the system is first quenched to 50 K, then equilibrated in the NpT ensemble, followed by further equilibration with NVT using periodic boundary conditions. Next, the CIs were adsorbed onto different locations of the surface, their structure was relaxed and heated to and equilibrated at 50 K after which production simulations followed.

All simulation environments used the flexible KKY model for water.³⁸ The implementation of the KKY model in CHARMM was that used in previous work.^{39,40} Droplets reminiscent

of aerosol particles were generated by starting from a cubic box of water containing 452 water molecules. Stochastic boundary conditions were applied to generate a droplet and for the duration of the simulations, water molecules were hindered to escape from the droplet by applying a center-of-mass constraint. These simulations used the KKY water model throughout. After preparation, the CIs were placed on top of the droplet surface. Heating and equilibration were carried out with a target temperature of 300 K. Following this, NVE simulations were carried out and the CIs remained unconstrained. In other words, the adsorbates were free to remain on top of the droplet, to diffuse into the droplet or to disengage from it.

For the simulations in solution, a solvent box with dimensions $40 \times 40 \times 40$ ų was generated using Packmol. The solute was placed into the center of the simulation box and remained there through application of a mild harmonic restraint (k = 1 kcal/mol/Ų) applied to the center-of-mass. Heating, equilibration and production dynamics were carried out at 300 K in the NVT ensemble. The long-range interactions were. The non-bonded forces between atoms separated by within 14 Å were computed, but smoothly switches them off between 10 and 12 Å.

MS-ARMD is a computationally efficient means to investigate chemical reactions. The force fields for the reactant and products were separately parameterized and the Gaussian and polynomial (GAPO) functions³⁴ were used to connect the reactant and product force fields to generate a continuous reactive PES along the reaction paths. On the other hand, PhysNet is a neural network that uses energies, forces, charges and dipole moments to minimize a loss function for obtaining a trained ML-PES. For H₂COO^{32,33} the CCSD(T)-F12a/aVTZ and CASPT2/aVTZ level of theories were used for calculating the reference datasets for fitting the MS-ARMD and PhysNet models, respectively, whereas for *syn*-CH₃CHOO, MP2/6-311++G(2d,2p) and CASPT2(12,10)/cc-pVDZ were used.³¹

Analysis

Structural and spectroscopic properties of the systems and the CIs were analyzed. The radial distribution functions g(r) were determined by using VMD.⁴¹ The IR spectra $I(\omega)$ were obtained via the Fourier transform of the dipole-dipole correlation function from the dipole moment time series

$$I(\omega)n(\omega) \propto Q(\omega) \cdot \operatorname{Im} \int_0^\infty dt \, e^{i\omega t} \sum_{i=x,y,z} \langle \boldsymbol{\mu}_i(t) \cdot \boldsymbol{\mu}_i(0) \rangle$$
 (1)

A quantum correction factor $Q(\omega) = \omega(1 - exp(-\beta\hbar\omega))$ was applied to the results of the Fourier transform.⁴²

Results

The structures of the two Criegee intermediates considered here are shown in Figure 1. For both CIs, H₂COO and syn-CH₃CHOO, the IR spectra were studied experimentally in the gas phase. ^{43,44} However, no data is available for the spectroscopy in solution, although some computational studies focused on the stability ⁴⁵ and new reaction mechanisms which leads to a new product HOCH₂OOH in bulk water. ⁴⁶

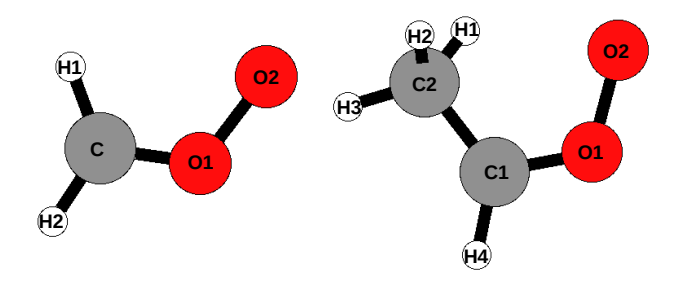


Figure 1: The structures of two Criegee intermediates, H₂COO and *syn*-CH₃CHOO, with atoms labelled.

The PESs used in the present work were previously validated vis-a-vis experimental mea-

surements. For the "small CI" (s-CI, H_2COO) this included the vibrational spectrum, ⁴³ the lifetime of the activated molecule and the fragmentation channels. ^{47,48} In particular, the recently trained ML-PES ³³ successfully identified the HCO+OH dissociation product as the "minority channel". Also, the computed vibrational frequencies including anharmonic corrections and mode-coupling are in reasonably good agreement with the experimental data. One difficulty in directly comparing measured and computed frequencies is in the challenging experimental characterization. The IR spectra for both, s-CI and l-CI, were not determined on pure samples but needed to be extracted from spectroscopic measurements of a reaction mixture through subtraction of other species' spectra, including CH_2I_2 , N_2 , O_2 , dioxirane, methylenebis(oxy), and cis-CH₂IOO. ^{43,44} Table S1 compares computed harmonic frequencies with experimentally assigned data for H_2COO . ⁴³ For the framework modes (below 2000 cm⁻¹), anharmonic corrections are estimated to be on the ~ 10 to ~ 50 cm⁻¹ depending on the mode considered. ^{33,48}

For the larger (l-CI, syn-Criegee) the energy-dependent rates and final vibrational and rotational state distributions of the OH-fragment were in excellent agreement with measurements. ^{30,31,49} For the computed vibrational frequencies compared with measurements the same remarks as for the s-CI above apply. Table S2 indicates that the computed harmonic frequencies using the ML-PES are in acceptable agreement with those reported from the experiments. Including anharmonic corrections will improve this comparison but is not done in the present work also because the data to compare with from experiment has some uncertainty. Hence, for both systems vetted MS-ARMD- and ML-PESs are available and used in the following.

Structure of the Water Environment

Next, the structure of the solvent molecules around the two CIs together with the water droplets was characterized. Figure 2 reports various radial distribution functions for H₂COO adsorbed to and within water droplets. Solid and dashed lines refer to the average and 20 individual MD trajectories run with the MS-ARMD (red) and ML-PES (blue) energy functions, respectively. The water structuring around C_{CI} (panel A), the droplet structure (panel B), and the water structure around the center of mass of H₂COO (panel C) are virtually identical for both PESs. On the other hand, using the center of mass separation between the droplet and the guest molecule, some differences are found (panel D). Towards the droplet surface $(r_{\text{CoM}_{\text{Water}}-\text{CoM}_{\text{CI}}} > 7.5 \text{ Å})$ the structures are comparable. The radial pair distributions for O_W-C_{CI}, O_W-O_W, O_W-CoM_{CI} are well converged for each individual simulation, giving nearly identical results (Panels A-C). However, when using the relative positioning of the centers of mass of the droplet and the CI (CoM_{droplet}-CoM_{CI}), the scatter is wider and for a converged average a larger number of independent simulations will be required. The individual g(r) in Figure 2D indicate that the CI can move between inside and surface sites. Figure S1 reports individual radial distribution functions for an inside position (using the MS-ARMD PES) and a surface position (using the ML-PES). It is found that the droplet structure is nearly identical (panel B), whereas the other three distribution functions differ to smaller or greater extents (panels A, C, D).

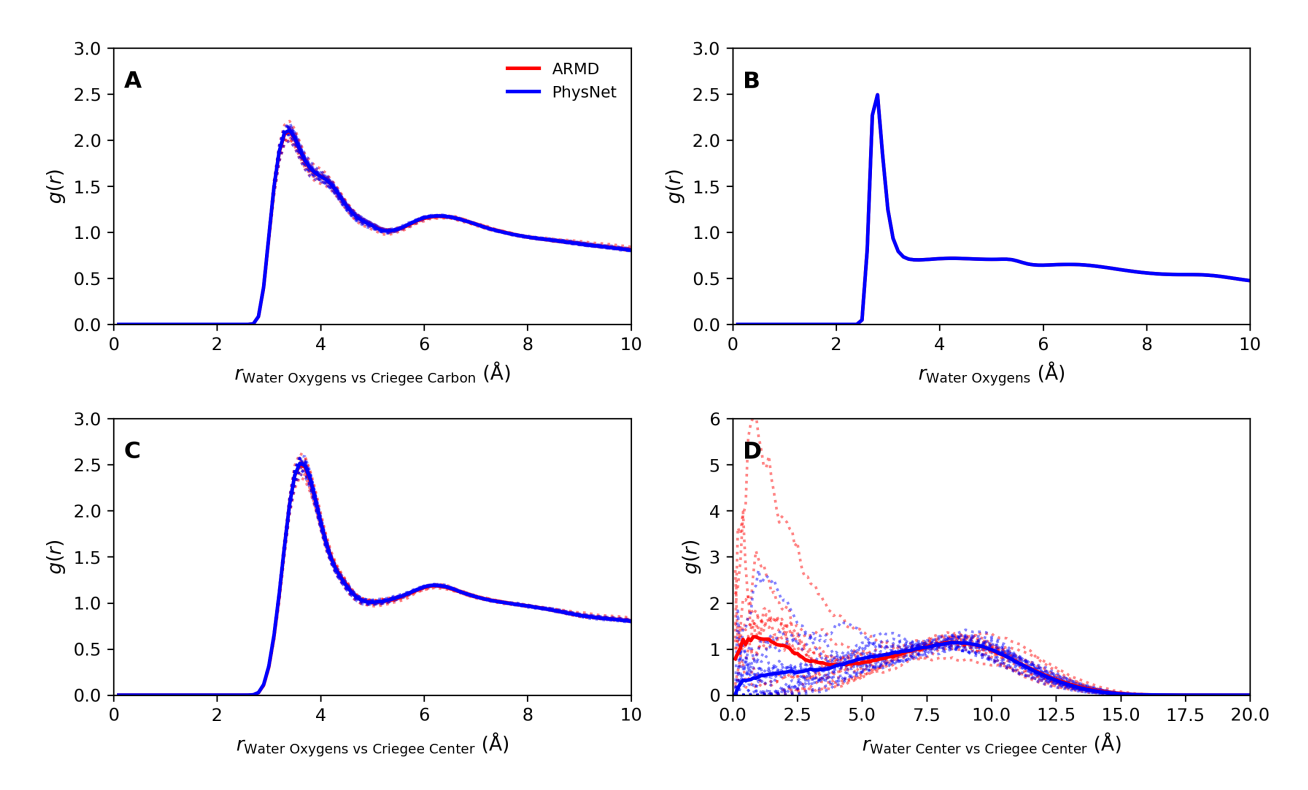


Figure 2: Radial pair distribution function for H_2COO (CI) on the water droplets. The radial distances in panels A to D are the O_W-C_{CI} , O_W-O_W , O_W-CoM_{CI} , and $CoM_{droplet}-CoM_{CI}$ separations. Averages over 20 independent simulations, each 2 ns in length, are shown for MS-ARMD (red thick lines) and PhysNet (blue thick lines) energy functions for H_2COO , respectively. Radial distribution functions for individual trajectories are shown as dotted lines. The two extreme cases, CI located inside the water droplet and adsorbed on its surface are shown in Figure S1.

Figure 3 reports two structures for H₂COO and syn-CH₃CHOO attached to the droplet surface. It is found that the guest molecule can fully insert despite the apolar CH₂-group. The partial atomic charges used in the MS-ARMD energy function are: C(0.313e), H1(0.205e), H2(0.192e), O1(-0.174e), and O2(-0.536e) (see Figure 1 for labels). Hence, the possibility for insertion is primarily driven by the hydration of the two oxygen atoms which form hydrogen bonds with the droplet-water molecules. Figure 3 also shows that the water droplet is not always perfectly spherical.

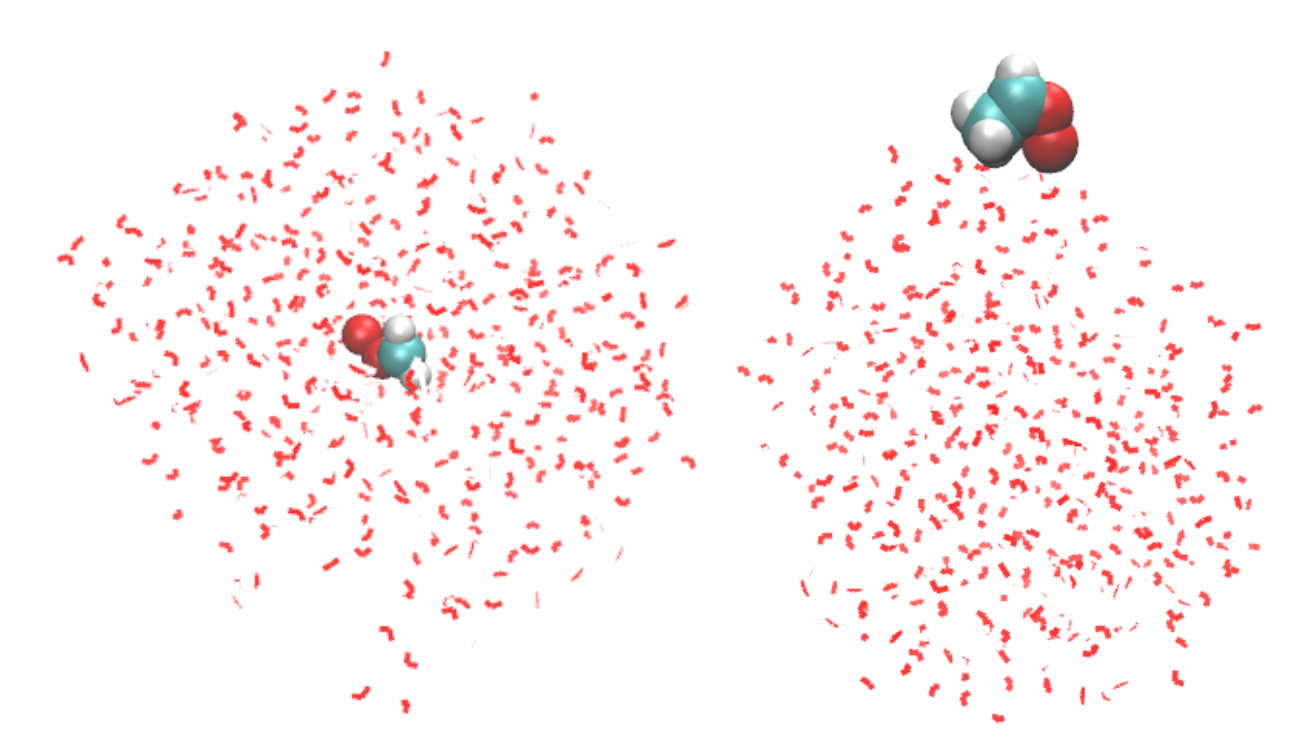


Figure 3: Snapshots of the droplet simulations with H_2COO (left) and syn-CH₃CHOO (right) as the guest molecule.

For syn-CH₃CHOO (see Figure 4), all three radial distribution functions involving the CI differ (panels A, C, D). The first peak for g(r) with $r_{\text{Ow-CCI}}$ is more intense if the MS-ARMD energy function is used in the simulations. For the $O_{\text{W-COM}_{\text{CI}}}$ separation as the relevant coordinate (Figure 4C) the radial distribution functions are closely overlapping whereas for the $r_{\text{CoM}_{\text{Water-CoM}_{\text{CI}}}}$ differences are largest. With the MS-ARMD energy function (red traces), syn-CH₃CHOO prefers to reside near the droplet surface whereas using the ML-PES, g(r) plateaus up to $r \sim 10$ Å after which it decays (blue traces). Considering individual trajectories (dotted lines), the differences between the two energy functions become even more apparent.

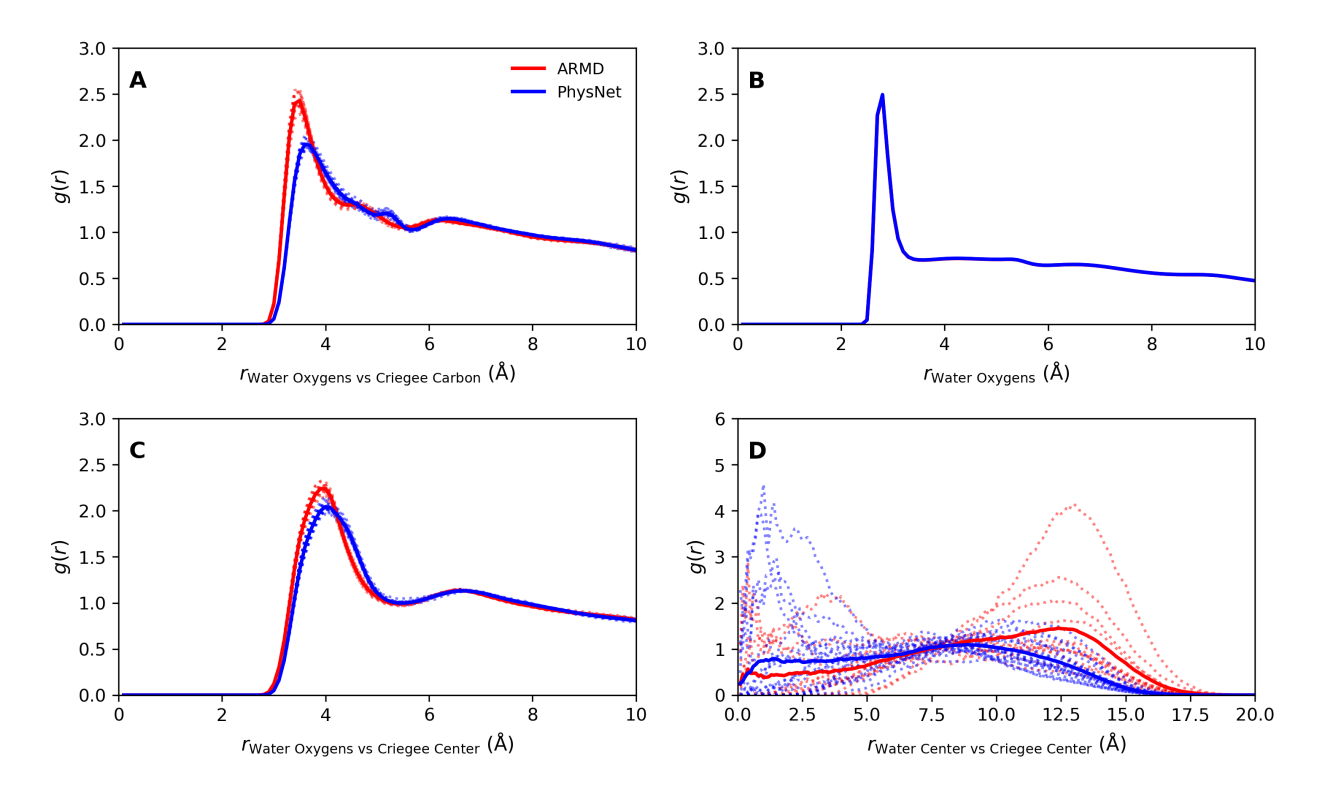


Figure 4: Radial pair distribution function for syn-CH₃CHOO (CI) on the water droplets. The radial distances in panels A to D are the O_W -C_{CI}, O_W -O_W, O_W -CoM_{CI}, and $CoM_{droplet}$ -CoM_{CI} separations. Averages over 20 independent simulations, each 2 ns in length, are shown for MS-ARMD (red thick lines) and PhysNet (blue thick lines) energy functions for syn-CH₃CHOO, respectively. Radial distribution functions for individual trajectories are shown as dotted lines.

For both CIs on the surface of ASW the motional freedom is rather restricted due to the low temperature at which the simulations were carried out (50 K). The CoM of both CIs remains close to its initial position on the 2 ns time scale although diffusion to neighboring sites would be possible in principle. Typical locations for the CoM_{CI} are indicated as orange point clouds in Figure 5. Surface diffusion for atoms and diatomic molecules involves barriers up to a few kcal/mol. As an example, experimentally and computationally estimated diffusion barriers for CO on ASW ranged from 0.25 to 1.85 kcal/mol. ^{50–53} Evidently, these diffusional barriers are higher for the two CIs.

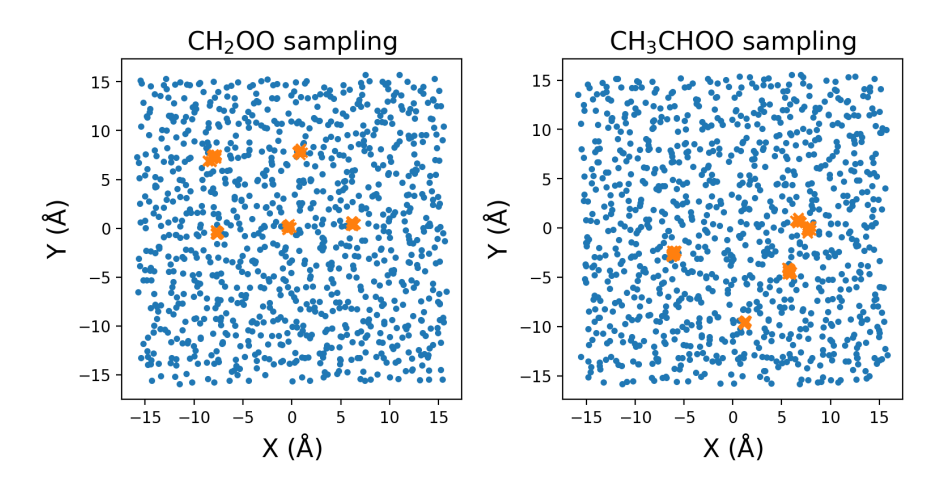


Figure 5: The CoM of CI sampled from 2 ns MD simulations at 50 K. The water molecules are free to move but only oscillate around their positions at such low temperature. The CIs are free to move but do not diffuse between neighboring wells at the low temperatures on short time scales.

Infrared Spectroscopy of CIs in Different Environments

Next, the IR spectra for both CIs in the gas phase and the different environments are presented and discussed, see Figures 6 and 7. As a reference, the averaged gas phase IR spectrum was determined from 20 independent trajectories, see panels A/E in Figures 6 and 7. For H₂COO three framework modes (below 2000 cm⁻¹) and one high-frequency mode were selected, see dashed vertical lines in Figure 6. From left to right, each dashed vertical line corresponds to the C-O-O scissor, O-O stretch, C-O stretch/H-C-H scissor, asymmetric C-H stretch modes in the left panels and C-O-O scissor, C-O stretch scissor, H-C-H scissor, asymmetric C-H stretch in the right panels. Approximate mode assignments are also given in Table S1.

All modes experience more or less pronounced environment-induced spectral shifts. Simulations using the MS-ARMD PES shift the mode at 511 cm⁻¹ by ~ 30 cm⁻¹ to the blue in

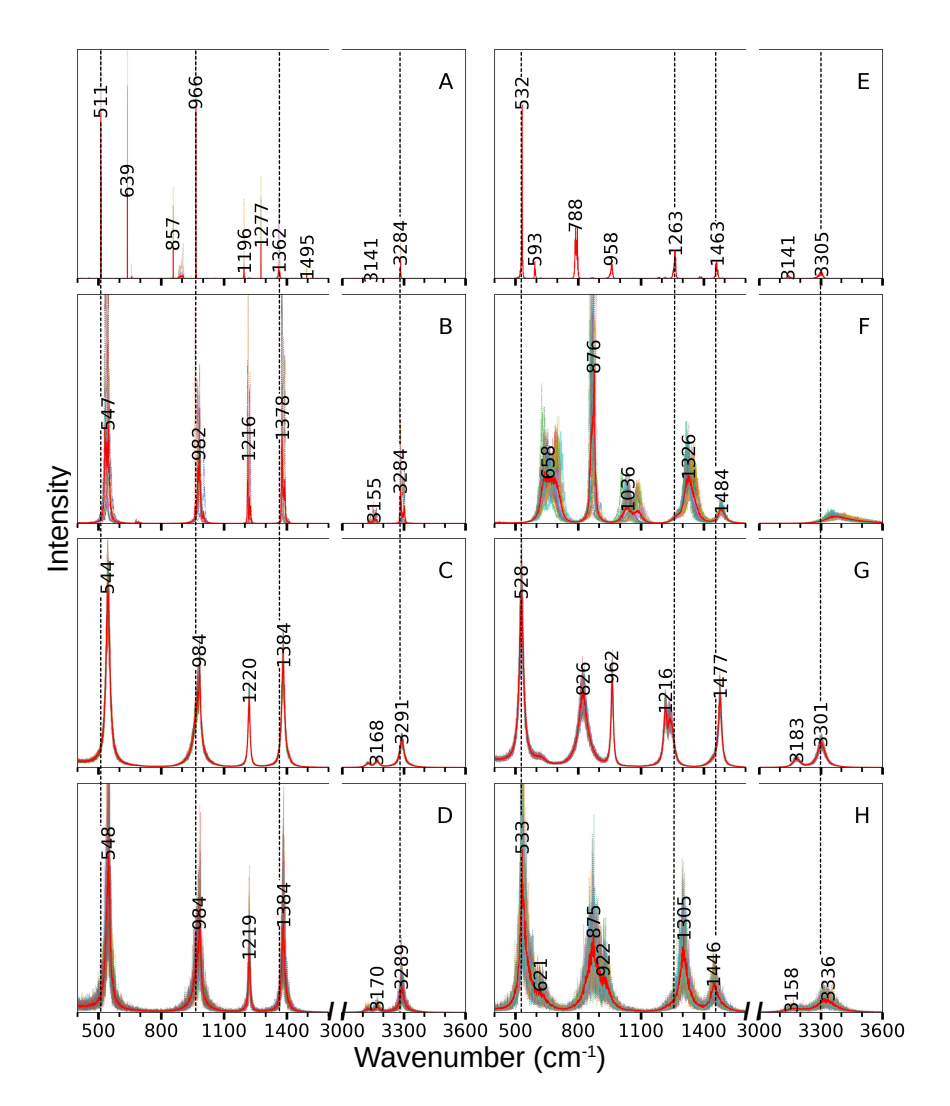


Figure 6: Simulated IR spectrum of H₂COO in four environments. Spectra from individual simulations and their average are the dotted and solid lines, respectively. for each case were. Pronounced peaks in the averaged spectra are labelled with the respective wavenumber. Panels A to D for simulations using the MS-ARMD energy function. Panels E to H for simulations using the ML-PES. Panels A/E, B/F, C/G, and D/H for simulations in the gas phase, on ASW, on/in water droplets, and in bulk water.

panels B to D. This is comparable to the 966 cm⁻¹ mode whereas the 1362 cm⁻¹ shifts rather by $\sim 20 \text{ cm}^{-1}$ to the blue. The blue shifts for the high-frequency CH-stretch mode is only $\sim 10 \text{ cm}^{-1}$. For simulations using the ML-PES (panels E to H) frequency shifts are observed as well. For this, the [532, 1263, 1463, 3305] cm⁻¹ modes were considered. The patterns of frequency shifts differs considerably from using the empirical MS-ARMD PES. Both, blue and red shifts are observed and some motions do not occur at all. For example, on ASW the

 532 cm^{-1} is entirely absent, whereas in/on the water droplet and in bulk water the mode shifts to the red by -4 cm^{-1} and to the blue by 1 cm^{-1} , respectively. Similar observations are made for the other modes considered.

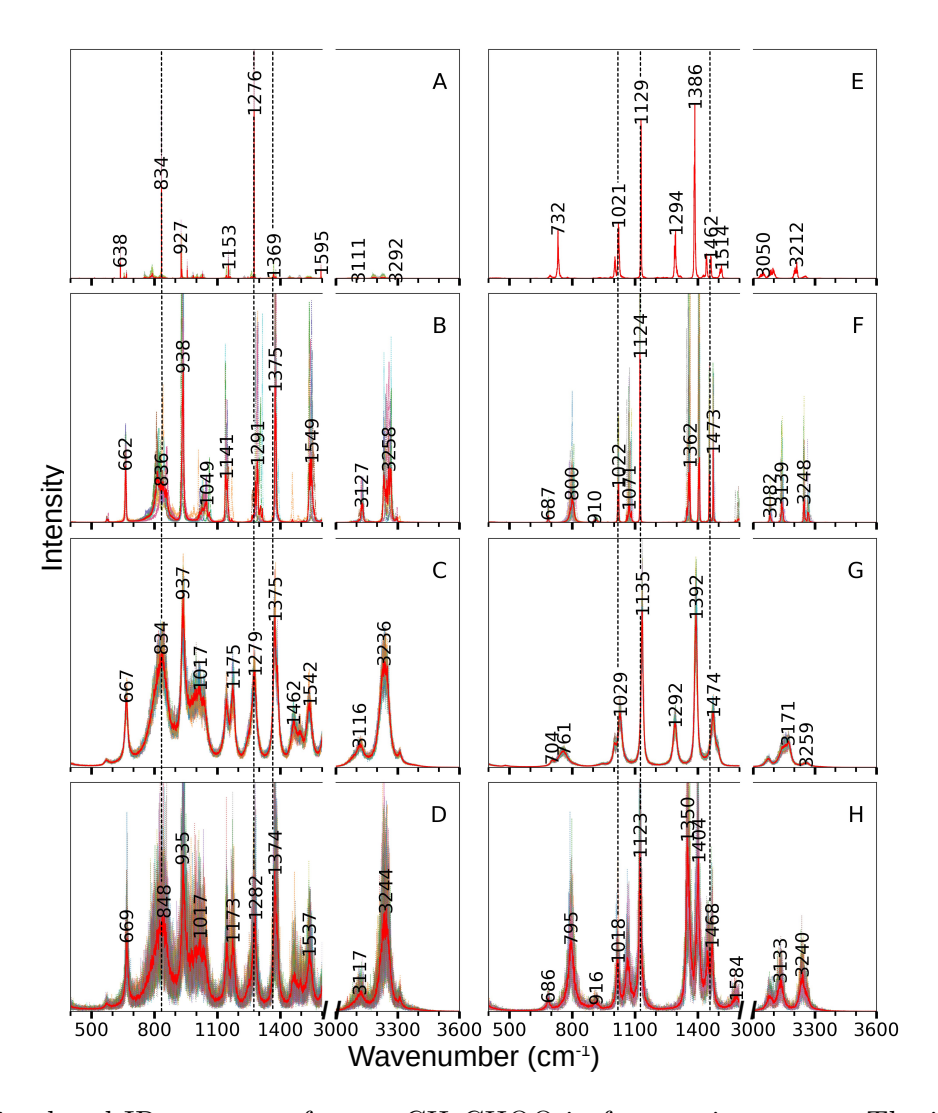


Figure 7: Simulated IR spectrum for syn-CH₃CHOO in four environments. The independent simulations for each case were presented with dotted lines and the average was presented with a red solid line. Pronounced peaks in the averaged spectra are labelled with the respective wavenumber. Panels A to D for simulations using the MS-ARMD energy function. Panels E to H for simulations using the ML-PES. Panels A/E, B/F, C/G, and D/H for simulations in the gas phase, on ASW, on/in water droplets, and in bulk water.

For the l-CI the findings follow those for H₂COO in that all environments lead to more or less pronounced frequency shifts relative to the gas phase. Typically, using the MS-ARMD energy

function leads to blue shifts: the 834 cm⁻¹ signal from the gas phase appears at [836, 834, 848] cm⁻¹ (ASW, droplet, bulk) whereas for the 1276 cm⁻¹ peak the different environments lead to [1291, 1279, 1282] cm⁻¹ signatures which are all shifted to the blue, see Figure 7A/D. As for the s-CI, the ML-PES leads to blue- as well as red-shifts. One example concerns the 1021 cm⁻¹ peak which shifts to [1022, 1029, 1018] cm⁻¹.

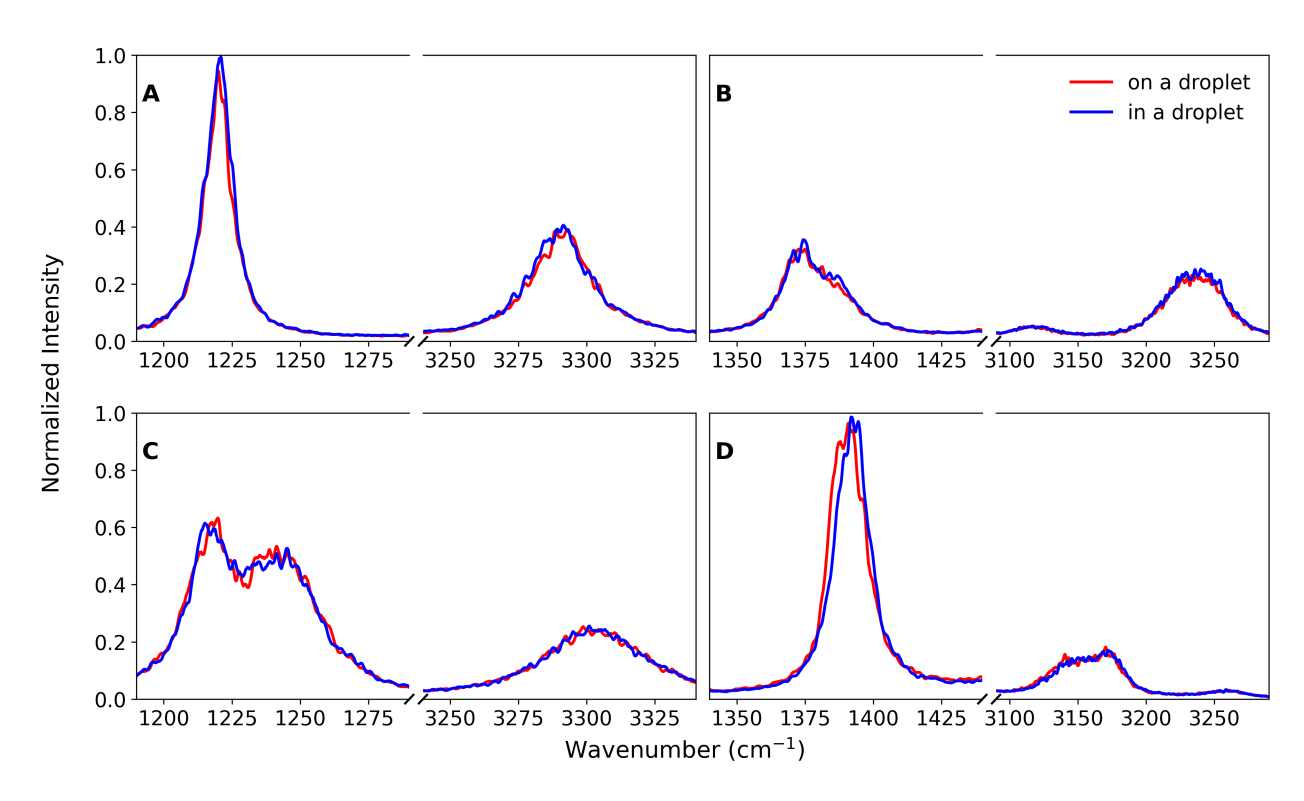


Figure 8: Comparison of IR spectrum with H₂COO (panels A and C) and syn-CH₃CHOO (panels B and D) on the droplet surface vs. inside the droplet. Top and bottom panels are from simulations using the MS-ARMD and ML-PES, respectively.

Since for the water droplet the s-CI and l-CI host molecules can reside either on the surface or within the droplet, it is also of interest to investigate whether the IR spectra between these two situations differ. An overview of the spectra for both CIs is given in Figures S2 and S3 using both PESs. The difference spectra (green) indicate that for both guest molecules the differences in the spectroscopy between adsorbed and inserted species are small.

For a more detailed analysis, individual spectral features were selected, see Figure 8. Inde-

pendent of the energy function used - MS-ARMD (panels A, B) or PhysNet (panels C, D) - the spectra with the s-CI or l-CI inside (blue) or on the surface (red) of the droplet only differ marginally. For the l-CI, using the MS-ARMD energy function, again no differences in the IR spectroscopy were found (Figure 8B) whereas using the ML-PES the framework mode around 1400 cm⁻¹ may respond slightly differently to the l-CI residing on the droplet (red) compared with the guest molecule being within the droplet (blue, shifted to higher frequency), see Figure 8D. For the high-frequency CH-stretch modes no differences between adsorbed and inserted guest molecule were found. It is possible that these findings change for larger droplets than those considered here, though.

Discussion and Conclusions

The present work considers the dynamics and spectroscopy of the two smallest Criegee intermediates, H₂COO and syn-CH₃CHOO, in the gas phase and in different hydration environments. For both systems, validated energy functions based on MS-ARMD and ML-based representations are available. The interest in environmental effects on the dynamics and spectroscopy derives primarily from the relevance of the two CIs in atmospheric chemistry where they can interact with water through adsorption on water droplets or water-microcrystals.

Most relevant for atmospheric chemistry are CIs in contact with water droplets. The present simulations find that both CIs can reside on the surface of droplets but also diffuse to the interior and stabilize there. The IR spectroscopy is largely independent on whether the CIs adsorb or insert. This is found for both PESs used in the present work. For the dynamics on ASW at low temperatures (50 K), both CIs remain at the initial adsorption sites.

Measurements are available for the two molecules in the gas phase whereas the spectroscopy

of CIs together with water droplets or ASW under laboratory conditions has not been reported so far. Typical measured reaction rates for CIs with water range from 10^{-13} cm³s⁻¹ to 10^{-16} cm³molecule⁻¹s⁻¹ which correspond to ~seconds and ~milliseconds depending on relative humidity for water densities of 10^{17} cm³ (high) and 10^{16} cm³ (low), respectively. ^{54,55} Hence, the lifetimes for CIs in contact with bulk water are sufficiently long that IR spectra can be obtained from either laboratory or earth-bound experiments. Computationally, the stability of s-CI and l-CI with one and two water molecules was determined. They range from ~ 2 kcal/mol to ~ 10 kcal/mol depending on the quantum chemical methods used. ^{45,46,56} Computed effective rates for the reaction of s-CI with two water molecules at 298 K and 20 % humidity were 10^4 s⁻¹. ⁴⁶ Given these findings it is anticipated that both, s-CI and l-CI, remain unreacted on the time scale of the present simulations (multiple-nanoseconds).

Overall, the present work finds that s-CI and l-CI can reside on top or within water droplets and their spectroscopy depends somewhat on the energy function used. With a MS-ARMD parametrization the spectral lines considered all remain unshifted or shift to the blue whereas the ML-PES leads to both, blue- and red-shifted features. One important difference between the two representations is that MS-ARMD is based on fixed point charges whereas the ML-PES (using the PhysNet architecture) includes geometry-dependent charges and it is anticipated that fluctuating charge models are better suited for quantitative studies. Importantly, using both PESs the magnitude of the spectral shifts between the gas-phase and in/on-droplet are consistent with typical Stark-induced red shifts from experiments and simulations in the condensed phase.

In conclusion, the spectroscopy of s-CI and l-CI in/on droplets and on ASW differs in characteristic ways from the gas-phase spectra but for the droplet sizes considered here, no differences for "inside" and "on surface" positions for droplets are found. On ASW the diffusional barriers are sufficiently high at low temperatures (50 K) to prevent surface

diffusion whereas for the droplets facile migration between "inside" and "on surface" positions is observed.

Acknowledgment

This work has been financially supported by the Swiss National Science Foundation (200021-117810, 200020-188724), and the University of Basel.

Supporting Information

The supporting material includes Tables with frequencies, additional radial distribution functions and comparisons between spectra for "inside" and "on surface" positions of s-CI and l-CI.

Data Availability

Relevant data for the present study are available at https://github.com/MMunibas/environment/.

References

- Pezzella, M.; Unke, O. T.; Meuwly, M. Molecular Oxygen Formation in Interstellar Ices
 Does Not Require Tunneling. J. Phys. Chem. Lett. 2018, 9, 1822–1826.
- (2) Lim, M.; Jackson, T. A.; Anfinrud, P. A. Binding of CO to myoglobin from a heme pocket docking site to form nearly linear Fe-C-O. *Science* **1995**, *269*, 962–966.
- (3) Lim, M.; Jackson, T. A.; Anfinrud, P. A. Mid-infrared vibrational spectrum of CO after photodissociation from heme: Evidence for a ligand docking site in the heme pocket of hemoglobin and myoglobin. J. Chem. Phys. 1995, 102, 4355–4366.
- (4) Lim, M.; Jackson, T. A.; Anfinrud, P. A. Ultrafast rotation and trapping of carbon monoxide dissociated from myoglobin. *Nat. Struct. Biol.* **1997**, *4*, 209–214.
- (5) Sagnella, D. E.; Straub, J. E.; Jackson, T. A.; Lim, M.; Anfinrud, P. A. Vibrational population relaxation of carbon monoxide in the heme pocket of photolyzed carbon-monoxy myoglobin: Comparison of time-resolved mid-IR absorbance experiments and molecular dynamics simulations. *Proc. Natl. Acad. Sci.* 1999, 96, 14324–14329.
- (6) Nutt, D. R.; Meuwly, M. Theoretical Investigation of Infrared Spectra and Pocket Dynamics of Photodissociated Carbonmonoxy Myoglobin. *Biophys. J.* 2003, 85, 3612–3623.
- (7) Nutt, D. R.; Meuwly, M. CO migration in native and mutant myoglobin: Atomistic simulations for the understanding of protein function. *Proc. Natl. Acad. Sci.* 2004, 101, 5998–6002.
- (8) Plattner, N.; Meuwly, M. The Role of Higher CO-Multipole Moments in Understanding the Dynamics of Photodissociated Carbonmonoxide in Myoglobin. *Biophys. J.* 2008, 94, 2505–2515.

- (9) Devereux, M.; Meuwly, M. Force Field Optimization using Dynamics and Ensemble Averaged Data: Vibrational Spectra and Relaxation in Bound MbCO. J. Chem. Inf. and Mod. 2010, 50, 90–99.
- (10) Suydam, I. T.; Snow, C. D.; Pande, V. S.; Boxer, S. G. Electric Fields at the Active Site of an Enzyme: Direct Comparison of Experiment with Theory. *Science* **2006**, *313*, 200–204.
- (11) Mondal, P.; Meuwly, M. Vibrational Stark spectroscopy for assessing ligand-binding strengths in a protein. *Phys. Chem. Chem. Phys.* **2017**, *19*, 16131–16141.
- (12) Xiong, H.; Lee, J. K.; Zare, R. N.; Min, W. Strong Electric Field Observed at the Interface of Aqueous Microdroplets. *J. Phys. Chem. Lett.* **2020**, *11*, 7423–7428.
- (13) Yan, X.; Bain, R. M.; Cooks, R. G. Organic reactions in microdroplets: Reaction acceleration revealed by mass spectrometry. Angew. Chem. Int. Ed. 2016, 55, 12960– 12972.
- (14) Banerjee, S.; Gnanamani, E.; Yan, X.; Zare, R. N. Can all bulk-phase reactions be accelerated in microdroplets? *Analyst* **2017**, *142*, 1399–1402.
- (15) Wei, Z.; Li, Y.; Cooks, R. G.; Yan, X. Accelerated reaction kinetics in microdroplets: Overview and recent developments. *Ann. Rev. Phys. Chem.* **2020**, *71*, 31–51.
- (16) Kappes, K. J.; Deal, A. M.; Jespersen, M. F.; Blair, S. L.; Doussin, J.-F.; Cazaunau, M.; Pangui, E.; Hopper, B. N.; Johnson, M. S.; Vaida, V. Chemistry and photochemistry of pyruvic acid at the air–water interface. J. Phys. Chem. A 2021, 125, 1036–1049.
- (17) Chhantyal-Pun, R.; Taatjes, C. A.; Percival, C. J. Direct Measurements of Conformer-Dependent Reactivity of the Criegee Intermediate CH₃CHOO. Nat. Chem. 2017, 9, 477–483.

- (18) Criegee, R.; Wenner, G. Die Ozonisierung des 9, 10-Oktalins. *Justus Liebigs Ann. Chem.* **1949**, *564*, 9–15.
- (19) Alam, M. S.; Camredon, M.; Rickard, A. R.; Carr, T.; Wyche, K. P.; Hornsby, K. E.; Monks, P. S.; Bloss, W. J. Total radical yields from tropospheric ethene ozonolysis. *Phys. Chem. Chem. Phys.* 2011, 13, 11002–11015.
- (20) Novelli, A.; Vereecken, L.; Lelieveld, J.; Harder, H. Direct observation of OH formation from stabilised Criegee intermediates. *Phys. Chem. Chem. Phys.* **2014**, *16*, 19941–19951.
- (21) Taatjes, C. A. Criegee intermediates: What direct production and detection can teach us about reactions of carbonyl oxides. *Ann. Rev. Phys. Chem.* **2017**, *68*, 183–207.
- (22) Mauldin III, R.; Berndt, T.; Sipilä, M.; Paasonen, P.; Petäjä, T.; Kim, S.; Kurtén, T.; Stratmann, F.; Kerminen, V.-M.; Kulmala, M. A new atmospherically relevant oxidant of sulphur dioxide. *Nature* **2012**, *488*, 193–196.
- (23) Mao, J.; Kuwata, K. T. Theoretical Investigation of the Reaction of Criegee Intermediates with Water and Water Dimer. J. Phys. Chem. A 2013, 117, 10188–10198.
- (24) Kuwata, K. T.; Valin, L. C. Reactivity of syn-CH₃CHOO with H₂O Enhanced through a Roaming Mechanism in the Entrance Channel. J. Phys. Chem. A **2020**, 124, 146–155.
- (25) Sheps, L. Absolute Ultraviolet Absorption Spectrum of CH₃CHOO. *Phys. Chem. Chem. Phys.* **2017**, *19*, 21970–21979.
- (26) Brooks, B. R.; Brooks III, C. L.; MacKerell Jr., A. D.; Nilsson, L.; Petrella, R. J.; Roux, B.; Won, Y.; Archontis, G.; Bartels, C.; Boresch, S. et al. CHARMM: The Biomolecular Simulation Program. J. Comp. Chem. 2009, 30, 1545–1614.
- (27) Buckner, J.; Liu, X.; Chakravorty, A.; Wu, Y.; Cervantes, L. F.; Lai, T. T.; Brooks III, C. L. pyCHARMM: Embedding CHARMM Functionality in a Python Framework. J. Chem. Theo. Comp. 2023, in print.

- (28) Song, K.; Käser, S.; Töpfer, K.; Vazquez-Salazar, L. I.; Meuwly, M. PhysNet Meets CHARMM: A Framework for Routine Machine Learning/Molecular Mechanics Simulations. J. Chem. Phys. 2023, 159, 024125.
- (29) Hwang, W.; Austin, S. L.; Blondel, A.; Boittier, E. D.; Boresch, S.; Buck, M.; Buckner, J.; Caflisch, A.; Chang, H.; Cheng, X. et al. CHARMM at 45: Enhancements in Accessibility, Functionality, and Speed. *J. Phys. Chem. B* **2024**, *128*, 9976–10042.
- (30) Upadhyay, M.; Meuwly, M. Thermal and vibrationally activated decomposition of the syn-CH₃CHOO Criegee intermediate. ACS Earth Space Chem. **2021**, 5, 3396–3406.
- (31) Upadhyay, M.; Töpfer, K.; Meuwly, M. Molecular Simulation for Atmospheric Reactions: Non-Equilibrium Dynamics, Roaming, and Glycolaldehyde Formation following Photoinduced Decomposition of syn-Acetaldehyde Oxide. *J. Phys. Chem. Lett.* 15, 90–96.
- (32) Song, K.; Upadhyay, M.; Meuwly, M. OH-Formation following vibrationally induced reaction dynamics of H₂COO. *Phys. Chem. Chem. Phys.* **2024**, *26*, 12698–12708.
- (33) Yin, C.; Käser, S.; Upadhyay, M.; Meuwly, M. Photodissociation Dynamics of Energized H₂COO: Formation of Molecular Products. J. Chem. Phys. **2025**, in print.
- (34) Nagy, T.; Yosa Reyes, J.; Meuwly, M. Multisurface adiabatic reactive molecular dynamics. *J. Chem. Theory Comput.* **2014**, *10*, 1366–1375.
- (35) Unke, O. T.; Meuwly, M. PhysNet: A neural network for predicting energies, forces, dipole moments, and partial charges. *J. Chem. Theory Comput.* **2019**, *15*, 3678–3693.
- (36) Lee, M. W.; Meuwly, M. Diffusion of atomic oxygen relevant to water formation in amorphous interstellar ices. *Faraday Discuss.* **2014**, *168*, 171–186.
- (37) Jorgensen, W. L.; Chandrasekhar, J.; Madura, J. D.; Impey, R. W.; Klein, M. L.

- Comparison of Simple Potential Functions for Simulating Liquid Water. *J. Chem. Phys.* **1983**, *79*, 926–935.
- (38) Kumagai, N.; Kawamura, K.; Yokokawa, T. An interatomic potential model for H₂O: Applications to water and ice polymorphs. *Mol. Sim.* **1994**, *12*, 177–186.
- (39) Plattner, N.; Meuwly, M. Atomistic Simulations of CO Vibrations in Ices Relevant to Astrochemistry. *ChemPhysChem* **2008**, *9*, 1271–1277.
- (40) Pezzella, M.; Meuwly, M. O₂ formation in cold environments. Phys. Chem. Chem. Phys. 2019, 21, 5559–5571.
- (41) Humphrey, W.; Dalke, A.; Schulten, K. VMD: visual molecular dynamics. J. Mol. Graph. 1996, 14, 33–38.
- (42) Ramírez, R.; López-Ciudad, T.; Kumar P, P.; Marx, D. Quantum corrections to classical time-correlation functions: Hydrogen bonding and anharmonic floppy modes. *J. Chem. Phys.* **2004**, *121*, 3973–3983.
- (43) Su, Y.-T.; Huang, Y.-H.; Witek, H. A.; Lee, Y.-P. Infrared absorption spectrum of the simplest Criegee intermediate CH₂OO. *Science* **2013**, *340*, 174–176.
- (44) Lin, H.-Y.; Huang, Y.-H.; Wang, X.; Bowman, J. M.; Nishimura, Y.; Witek, H. A.; Lee, Y.-P. Infrared identification of the Criegee intermediates *syn*-and *anti*-CH₃CHOO, and their distinct conformation-dependent reactivity. *Nat. Commun.* **2015**, *6*, 7012.
- (45) Zhong, J.; Kumar, M.; Zhu, C. Q.; Francisco, J. S.; Zeng, X. C. Surprising stability of larger Criegee intermediates on aqueous interfaces. Angew. Chem. Int. Ed. 2017, 56, 7740–7744.
- (46) Zhu, C.; Kumar, M.; Zhong, J.; Li, L.; Francisco, J. S.; Zeng, X. C. New mechanistic pathways for Criegee–water chemistry at the air/water interface. *J. Am. Chem. Soc.* **2016**, *138*, 11164–11169.

- (47) Nguyen, T. L.; Lee, H.; Matthews, D. A.; McCarthy, M. C.; Stanton, J. F. Stabilization of the simplest Criegee intermediate from the reaction between ozone and ethylene: A high-level quantum chemical and kinetic analysis of ozonolysis. *J. Phys. Chem. A* **2015**, 119, 5524–5533.
- (48) Qian, Y.; Nguyen, T. L.; Franke, P. R.; Stanton, J. F.; Lester, M. I. Nonstatistical Unimolecular Decay of the CH₂OO Criegee Intermediate in the Tunneling Regime. *J. Phys. Chem. Lett.* **2024**, *15*, 6222–6229.
- (49) Kidwell, N. M.; Li, H.; Wang, X.; Bowman, J. M.; Lester, M. I. Unimolecular dissociation dynamics of vibrationally activated CH₃CHOO Criegee intermediates to OH radical products. Nat. Chem. 2016, 8, 509–514.
- (50) Karssemeijer, L.; Cuppen, H. Diffusion-desorption ratio of adsorbed CO and CO₂ on water ice. *Astron. Astrophys.* **2014**, *569*, A107.
- (51) Kouchi, A.; Furuya, K.; Hama, T.; Chigai, T.; Kozasa, T.; Watanabe, N. Direct Measurements of Activation Energies for Surface Diffusion of CO and CO₂ on Amorphous Solid Water Using In Situ Transmission Electron Microscopy. Astrophys. J. Lett. 2020, 891, L22.
- (52) Acharyya, K. Understanding the impact of diffusion of CO in the astrochemical models. *Pub. Astron. Soc. Austr.* **2022**, *39*, e009.
- (53) Upadhyay, M.; Meuwly, M. CO₂ and NO₂ formation on amorphous solid water. *Astron. Astrophys.* **2024**, *689*, A319.
- (54) Taatjes, C. A.; Welz, O.; Eskola, A. J.; Savee, J. D.; Scheer, A. M.; Shallcross, D. E.; Rotavera, B.; Lee, E. P. F.; Dyke, J. M.; Mok, D. K. W. et al. Direct measurements of conformer-dependent reactivity of the Criegee intermediate CH₃CHOO. Science 2013, 340, 177–180.

- (55) Liu, Y.; Liu, L.; Fu, Y.; Jiang, H.; Wu, H.; Liu, Y.; Lu, X.; Zhou, X.; Li, H.; Skodje, R. T. et al. Reactivity of syn-CH₂CHOO with H₂O enhanced through a roaming mechanism in the entrance channel. *Nat. Chem.* **2025**, *17*, 897–903.
- (56) Lin, L.-C.; Chang, H.-T.; Chang, C.-H.; Chao, W.; Smith, M. C.; Chang, C.-H.; Lin, J. J.-M.; Takahashi, K. Competition between H₂O and (H₂O)₂ reactions with CH₂OO/CH₃CHOO. *Phys. Chem. Chem. Phys.* **2016**, *18*, 4557–4568.

SUPPORTING INFORMATION: Structure and Spectroscopy of Criegee Intermediates in Gas- and Aqueous Environments

Tables

Table S1: Harmonic frequencies of H_2COO from the *ab initio* calculation, the resent PhysNet model, and experiment, ⁴³ in cm⁻¹.

Normal Modes	CASPT2/aVTZ	CCSD(T)-F12a/aVTZ	PhysNet	Exp^{43}
ν_1 : asymmetric C–H stretch	3328.37	3304.02	3333.66	
ν_2 : symmetric C–H stretch	3164.23	3144.62	3169.95	
ν_3 : H-C-H scissor	1487.95	1492.57	1486.44	1435
ν_4 : C-O stretch/H-C-H scissor	1273.88	1318.64	1285.72	1286
ν_5 : C–O stretch	1239.27	1244.46	1241.02	1241
ν_6 : O–O stretch	1001.58	952.36	966.13	908
ν_7 : H-C-H-rock	748.18	873.02	816.99	848
ν_8 : H-C-H-wag	630.72	650.04	612.74	
ν_9 : C-O-O scissor	543.26	539.67	554.63	

Table S2: Harmonic frequencies of syn-CH₃CHOO from the ab initio calculation and the available experiment measurement, 44 in cm⁻¹.

Normal Modes	MP2/aVTZ	MP2/6-311++G(2d,2p)	PhysNet	Exp^{44}
ν_1	3253.22	3286.83	3251.91	
$ u_2$	3208.70	3240.90	3207.67	
$ u_3$	3101.20	3146.18	3102.08	
$ u_4$	3047.81	3088.37	3048.12	
$ u_5$	1514.80	1531.36	1513.69	1477
$ u_6$	1474.35	1522.91	1474.24	
$ u_7$	1456.37	1500.14	1457.16	
$ u_8$	1397.69	1446.74	1397.50	
$ u_9$	1296.20	1298.27	1295.50	1281
$ u_{10}$	1130.54	1163.85	1129.79	1091
$ u_{11}$	1031.22	1052.81	1030.95	
$ u_{12}$	996.49	1013.63	995.86	956
$ u_{13}$	940.31	958.16	939.79	871
$ u_{14}$	745.36	721.75	744.90	
$ u_{15}$	698.64	709.42	698.19	
$ u_{16}$	480.98	470.49	481.11	
$ u_{17}$	303.96	310.34	308.88	
$ u_{18} $	224.63	216.80	223.27	

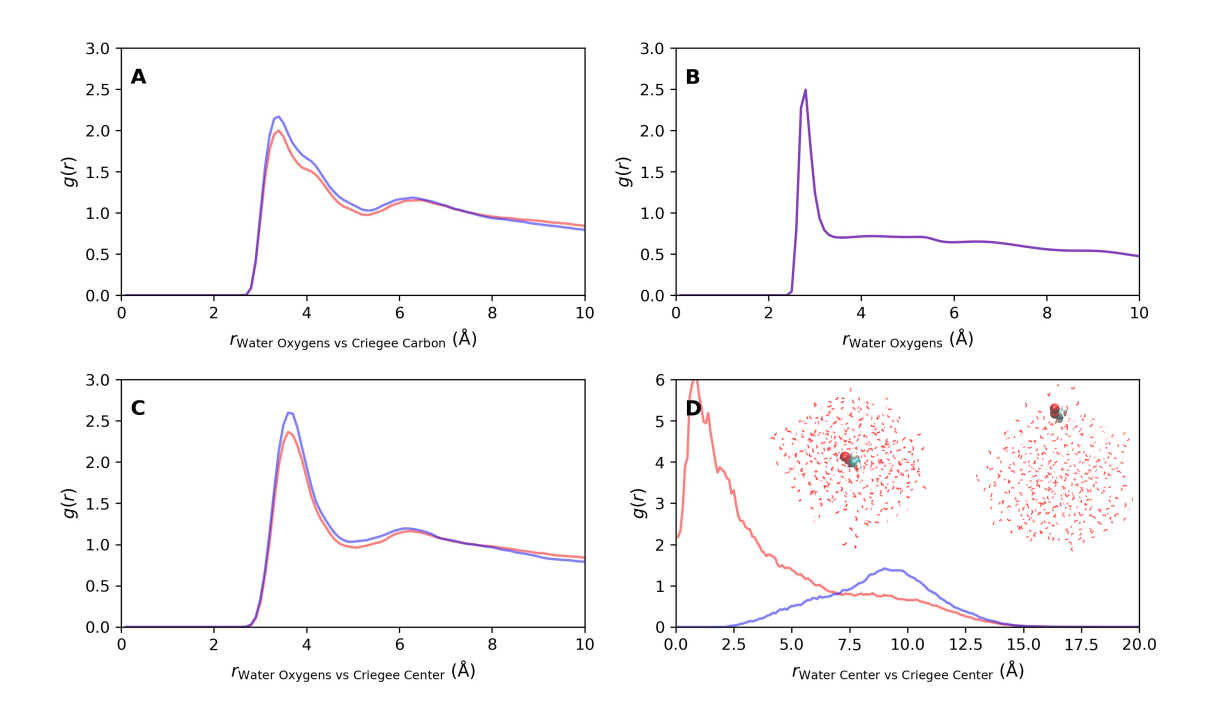


Figure S1: Radial pair distribution function for H_2COO (CI) on the water droplets. The radial distances in panels A to D are the O_W-C_{CI} , O_W-O_W , O_W-CoM_{CI} , and $CoM_{droplet}-CoM_{CI}$ separations. The data from MS-ARMD and PhysNet simulations are represented by red and blue curves, respectively. The insets provide snapshots illustrating the CI located inside the water droplet and adsorbed on its surface.

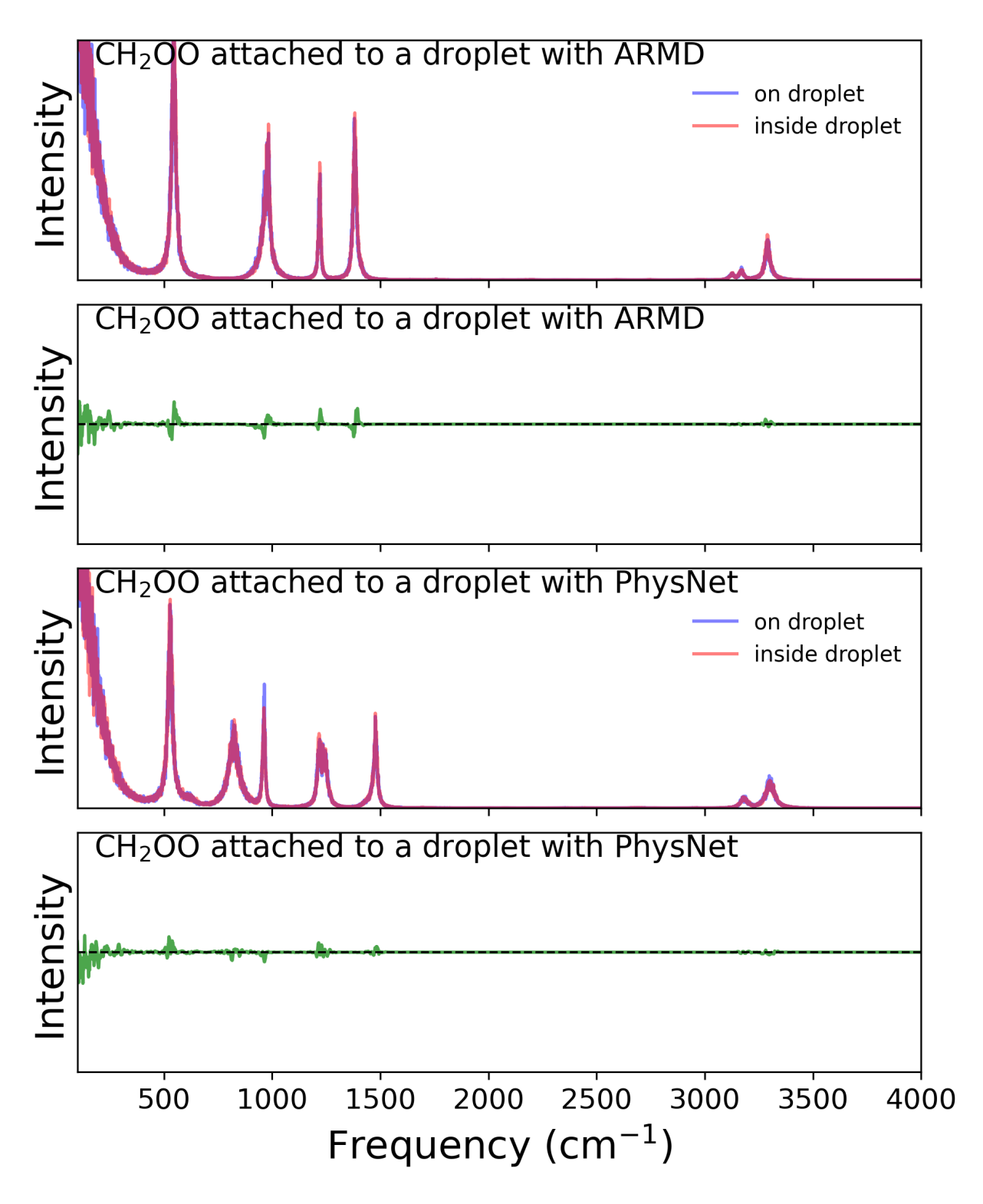


Figure S2: Comparison of IR spectrum of H_2COO between Criegee on the surface .vs. inside a droplet. The differences between the two cases are shown below.

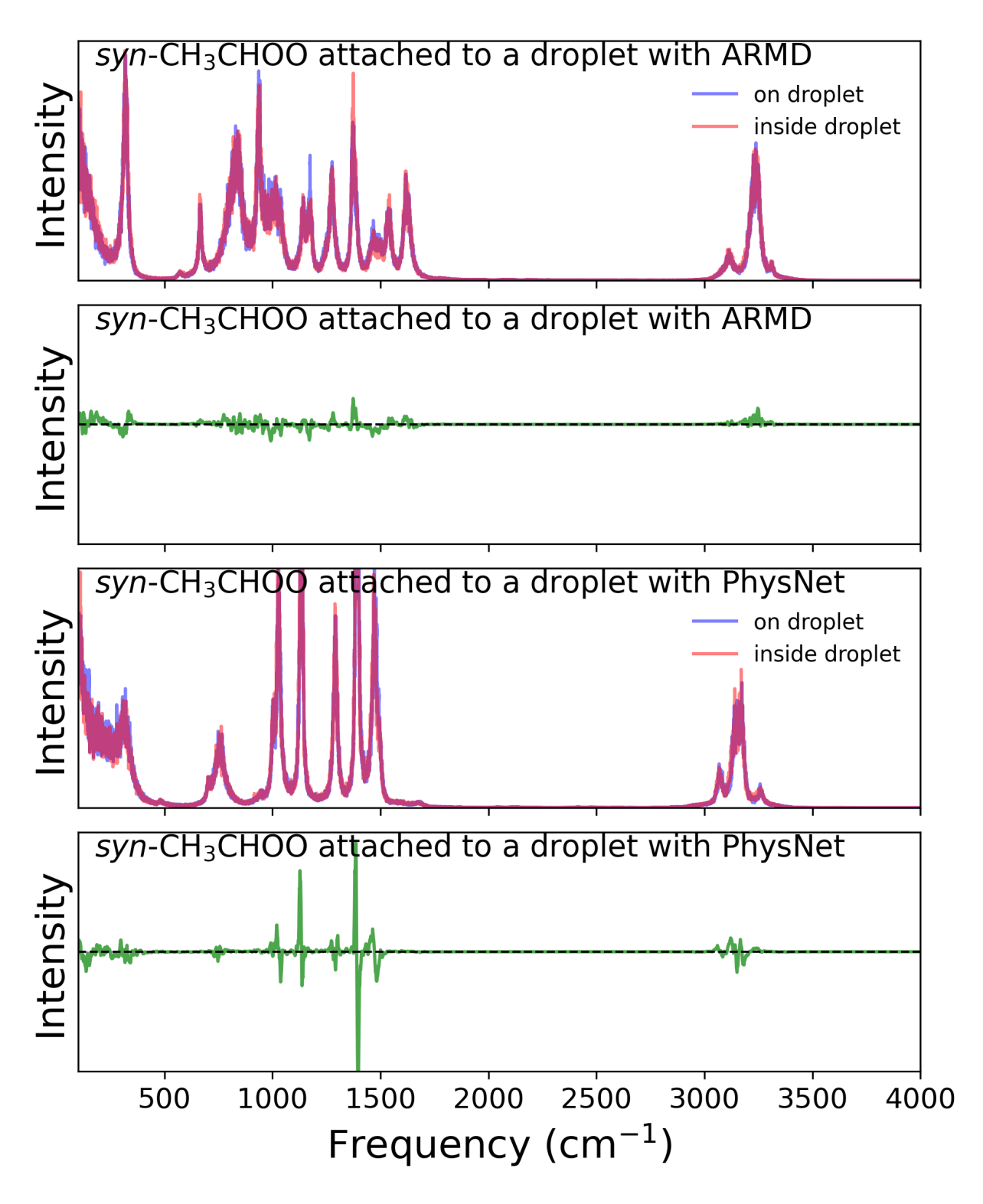


Figure S3: Comparison of IR spectrum of syn-CH₃CHOO between Criegee on the surface .vs. inside a droplet. The differences between the two cases are shown below.